Biochimica et Biophysica Acta 1838 (2014) 1010–1018

Contents lists available at ScienceDirect

Biochimica et Biophysica Acta

journal homepage: www.elsevier.com/locate/bbamem

Structural features of the C8 antiviral peptide in a membrane-mimicking environment

Mario Scrima [a], Sara Di Marino [b], Manuela Grimaldi [a], Federica Campana [a], Giuseppe Vitiello [b], Stefano Piotto Piotto [a], Gerardino D'Errico [b], Anna Maria D'Ursi [a,*]

[a] Department of Pharmacy, University of Salerno, Fisciano, Italy
[b] Department of Pharmacy, University of Naples "Federico II", Naples, Italy

ARTICLE INFO

Article history:
Received 3 September 2013
Received in revised form 12 December 2013
Accepted 16 December 2013
Available online 22 December 2013

Keywords:
NMR
Conformational analysis
Glycoprotein
Viral fusion

ABSTRACT

C8, a short peptide characterized by three regularly spaced Trp residues, belongs to the membrane-proximal external functional domains of the feline immunodeficiency virus coat protein gp36. It elicits antiviral activity as a result of blocking cell entry and exhibits membranotropic and fusogenic activities. Membrane-proximal external functional domains of virus coat proteins are potential targets in the development of new anti-HIV drugs that overcome the limitations of the current anti-retroviral therapy. In the present work, we studied the conformation of C8 and its interaction with micellar surfaces using circular dichroism, nuclear magnetic resonance and fluorescence spectroscopy. The experimental data were integrated by molecular dynamics simulations in a micelle–water system. Our data provide insight into the environmental conditions related to the presence of the fusogenic peptide C8 on zwitterionic or negatively charged membranes. The membrane charge modulates the conformational features of C8. A zwitterionic membrane surface induces C8 to assume canonical secondary structures, with hydrophobic interactions between the Trp residues and the phospholipid chains of the micelles. A negatively charged membrane surface favors disordered C8 conformations and unspecific superficial interactions, resulting in membrane destabilization.

1. Introduction

Human immunodeficiency virus (HIV) enters the target cell using fusion machinery composed of the non-covalently associated gp120 and gp41 glycoproteins. The formation of the fusion complex induces extensive conformational changes in gp120, resulting in the dissociation of the gp120/gp41 complex and the subsequent release of metastable gp41. Virus–cell fusion is then initiated by the gp41 ectodomain [1]. The gp41 ectodomain contains several characteristic functional domains, including the fusion peptide (FP), N-terminal heptad repeat (NHR), C-terminal heptad repeat (CHR) and membrane proximal extracellular region (MPER). The MPER is located at the C-terminal end of the HIV-1 gp41 ectodomain and is directly followed by the transmembrane domain. In the HIV-1 gp41 pre-hairpin structure, the MPER and the FP are the functional links by which the gp41 pre-hairpin bridges the viral and target cell membranes through the formation of a coiled-coil six-helix bundle (6HB) structure [2].

Fusion inhibitors that target gp41's functional domains to prevent 6HB formation and terminate the HIV-1-cell fusion process can be used as drugs to prevent HIV-1 infection.

In 2003, a 36-amino acid peptide derived from the CHR of the HIV-1 gp41 ectodomain (enfuvirtide T20) was approved by the US FDA for anti-HIV treatment. T20 is the only currently approved drug targeting gp41; however, the high cost and inconvenience of the twice daily injection of this peptide drug prevent it from being used as a regular anti-HIV drug [3]. The development of new fusion inhibitors that overcome the limitations of T20 is of great importance. The NHR and CHR are still the most intensively investigated targets in gp41 [4]. Other less exploited functional domains, such as the FP [5] and the MPER [6], are receiving increasing attention as potential targets for fusion inhibitors.

Feline immunodeficiency virus (FIV) is a naturally occurring lentivirus [7] that is studied as a model system for anti-HIV vaccines and anti-HIV drug development [8,9]. In a manner analogous to that for HIV, FIV enters cells via a mechanism involving a surface glycoprotein named gp36 [10–12]. Gp36 has a structural architecture similar to that of gp41. The MPER of gp36 has a crucial role in the membrane fusion process [7,13–15]. We previously demonstrated that several short synthetic peptides that mimic the MPER of gp36 [16,17] reduce the infectivity of FIV [18]. In particular, the fragment ^{770}WEDWVGWI^{776}, dubbed C8, elicited antiviral activity as a result of blocking cell entry, as observed for HIV fusion inhibitors [19,20]. A structure–activity-relationship (SAR) study and preliminary nuclear magnetic resonance (NMR) conformational analysis demonstrated that C8's antiviral activity depends on the presence of regularly spaced Trp residues and that the orientation

* Corresponding author at: Department of Pharmacy, University of Salerno, Via Giovanni Paolo II, 84084 Fisciano (Sa), Italy. Tel.: +39 089969748.
E-mail address: dursi@unisa.it (A.M. D'Ursi).

0005-2736/$ – see front matter © 2013 Elsevier B.V. All rights reserved.
http://dx.doi.org/10.1016/j.bbamem.2013.12.010

of the Trp indolyl rings is critical on a turn-shaped backbone conformations [21–25].

The antiviral activity based on blocking cell entry strongly supports the hypothesis that C8 has a direct interaction with the virus or the cell membrane; therefore, understanding these interactions may provide new insight into the mechanism of virus–cell fusion and may aid in the identification of new targets for FIV and HIV fusion inhibitors. With this in mind and given the hypothesis that the membrane's properties have profound effects on the fusion processes involving the FIV-1 gp36 ectodomain and beyond, C8 has been studied in membrane models of varying complexity and compositions using several spectroscopic techniques and molecular dynamics simulations [26,27]. Our data show that C8 adsorbs strongly to zwitterionic bilayer surfaces due to hydrogen bonds and hydrophobic interactions involving the Trp side chains and the lipid head groups. This interaction induces a decrease in the bilayer thickness and an increase in the hydration of the lipid head groups [28]. In dipalmitoylphosphatidylcholine (DPPC) bilayers containing cholesterol and sphingomyelin, the peptide-induced fusion mechanism requires a strict interplay among the different lipids [29].

The reported data, although acquired in highly sophisticated biomembrane environments, present only indirect information about C8's three-dimensional structure. Therefore, to develop a structural model of C8 in membrane mimetic conditions, in the present work we performed a conformational analysis using circular dichroism (CD) and NMR in micelle solutions of dodecylphosphocholine (DPC) and sodium dodecyl sulfate (SDS) detergents; these are accepted mimetics of negatively charged and zwitterionic bio-membranes respectively, suitable for NMR spectroscopy [30,31]. To study the positioning of C8 on the micelle surface, we used fluorescence spectroscopy, pulsed field gradient (PFG) NMR experiments and NMR measurements in the presence of spin labels. The experimental data were integrated by molecular dynamics calculations in a micelle–water system.

Our data show that membrane charge modulates the conformation of C8. Zwitterionic membrane surfaces induce a regular C8 conformation, with hydrophobic interactions occurring between Trp residues and the phospholipid chains. Negative charges favor C8 conformational flexibility and superficial interactions resulting in membrane destabilization. Information concerning the conformational preferences of C8 and its mode of interactions with micelle surfaces may be used in the design of new fusion inhibitors targeting the MPER.

2. Experimental section

2.1. Peptide synthesis

C8 peptide was prepared manually using a conventional solid-phase strategy with N-α-fluorenylmethoxycarbonyl-protected amino acids and a Rink-amide resin as a solid support. The peptide was N-terminally acetylated and C-terminally amidated to improve enzymatic stability. The crude peptide was purified to homogeneity by semipreparative reverse-phase high-pressure liquid chromatography, resulting in a purity greater than 95%, and then lyophilized. The final product was characterized by analytical high-pressure liquid chromatography and electrospray mass spectrometry [18].

2.2. Fluorescence spectroscopy

Fluorescence measurements were performed at 300 K using a LS55 Luminescence Spectrofluorimeter (Perkin Elmer). The excitation wavelength was 280 nm, and emission spectra were recorded between 310 and 450 nm with an excitation slit width of 5 nm, an emission slit width of 2.5 nm and a scan speed 50 nm/min. The titrations with SDS and DPC were performed by adding known amounts of a phosphate buffer solution (pH 7; 10 mM) containing the peptide (3×10^{-6} M) and the surfactant at a concentration well above the critical micelle concentration (c.m.c.) to a weighed amount of a phosphate buffer solution of the peptide with the same concentration, initially placed into the spectrofluorimetric cuvette. In this manner, the surfactant concentration was progressively increased while the peptide concentration remained constant during the whole titration. After each addition, there was a 10-min wait to ensure that equilibrium had been reached.

2.3. Circular dichroism spectroscopy

All CD spectra were recorded using a JASCO J810 spectropolarimeter at room temperature with a cell path length of 1 mm. CD spectra were acquired at 25 °C using a measurement range from 190 to 260 nm, a bandwidth of 1 nm, four accumulations and a scanning speed of 10 nm/min. During all the measurements, the trace of the high tension voltage was verified to be less than 700 V, which should ensure the reliability of the data obtained [32]. Spectra were corrected for the solvent contribution.

Samples containing the peptide (1×10^{-4} M) in phosphate buffer (pH 6.8, 25 mM) and increasing concentrations of DPC (0.6 mM, 1.2 mM, 5.0 mM and 10 mM) or SDS (4.0 mM, 8.0 mM, 40 mM and 80 mM) were prepared. Estimation of secondary structure content was performed using the algorithms CONTIN and SELCON from the DICHROWEB website [33].

2.4. NMR analysis

Samples for NMR experiments were prepared to have C8 1 mM, in mixture of DPC- or SDS-aqueous solution (pH 6.8 phosphate buffer containing H_2O/D_2O 90:10 v/v). C8 phosphate buffer solution was titrated with increasing amounts of d_{25}-SDS (4.0 mM, 8.0 mM, 40 mM and 80 mM) or d_{38}-DPC (0.6 mM, 1.2 mM, 5.0 mM and 10 mM) surfactant. 1D ^{1}H homonuclear spectra in the Fourier mode with quadrature detection were recorded at each step of the titration. Two-dimensional (2D) ^{1}H homonuclear TOCSY and NOESY spectra were recorded in the final micelle solutions containing 1.0 mM C8 and 10.0 mM DPC or 80.0 mM SDS respectively.

NMR spectra were recorded on a Bruker DRX-600 spectrometer. 2D ^{1}H homonuclear TOCSY and NOESY spectra were collected in the phase-sensitive mode using quadrature detection in $\omega 1$ by time-proportional phase incrementation of the initial pulse [34–36]. The water signal was suppressed using WATERGATE pulse sequence experiments [37]. The data block sizes were 2048 addresses in t_2 and 512 equidistant t_1 values. Before Fourier transformation, the time domain data matrices were multiplied by shifted $\sin^2$ functions in both dimensions. A mixing time of 70 ms was used for the TOCSY experiments. NOESY experiments were run at 300 K with mixing times in the range of 100–300 ms. Qualitative and quantitative analyses of DQF-COSY, TOCSY, and NOESY spectra were performed using SPARKY software [38].

NMR experiments in the presence of spin-probes were performed using a solution of 5-DSA spin-probes prepared using methanol-d_4 as the solvent. The spin-probes were added to deuterated SDS-d_{25} and DPC-d_{38} micellar solutions of C8 peptides at a spin-probe/micelle concentration ratio of 1:1.

2.5. NMR structure calculations

Peak volumes were translated into upper distance bounds with the CALIBA routine from the CYANA software package [39]. The requisite pseudoatom corrections were applied for non-stereospecifically assigned protons at pro-chiral centers and for the methyl group. After discarding redundant and duplicated constraints, the final list of experimental constraints was used to generate an ensemble of 100 structures with the standard CYANA protocol of simulated annealing in the torsion angle space (using 10,000 steps). No dihedral angle or hydrogen bond restraints were applied. The best 20 structures that had low target function values and small residual violations were refined by in vacuo

minimization in the AMBER 1991 force field using the SANDER program of the AMBER 5.0 suite [40,41]. To mimic the effect of solvent screening, all net charges were reduced to 20% of their real values. In addition, a distance-dependent dielectric constant ($\varepsilon = r$) was used. The cut-off for non-bonded interactions was 12 Å. NMR-derived upper bounds were imposed as semi-parabolic penalty functions, with force constants of 16 kcal/mol Å^2. The function was shifted to be linear when the violation exceeded 0.5 Å. The best 10 structures after minimization had AMBER energies ranging from −1541.4 to −1391.1 kcal/mol. The final structures were analyzed using the Insight 98.0 program (Molecular Simulations, San Diego, CA, USA).

2.6. PFG-NMR measurements of diffusion

Diffusion NMR measurements were performed using the PFG method on a Bruker DRX 500 spectrometer equipped with a z-gradient system capable of producing magnetic field pulse gradients of approximately 50 G cm^{-1} using a 5 mm inverse BBI probe. The bipolar phase longitudinal encode decode (BPP-LED) sequence developed by Johnson and coworkers [42,43] was used to determine the self-diffusion coefficient of C8 (i) in aqueous solution and (ii) in SDS or DPC micellar solutions. The surfactants' self-diffusion coefficients were also determined in the absence and the presence of the peptide. For each investigated sample, a series of twenty BPP-LED experiments was conducted with increasing gradient strength. The intensity of the observed signal is related to diffusion by

$$I_i = I_{0i} \exp\left[-D_i \gamma^2 g^2 \delta^2 (\Delta - \delta/3)\right] \quad (1)$$

where I_i is the intensity of the ith signal in the presence of the gradient pulses; I_{0i} is the intensity of the ith signal without the gradient pulses; γ is the magnetogyric ratio of the observed nucleus; δ and g are the gradient duration and strength, respectively; Δ is the distance between the leading edges of the gradient pulses (the diffusion time); and D_i is the diffusion coefficient of the ith species [42,44–46].

To determine I_i, each spectrum was integrated in a specific region that contained no overlapping signals. Accurate values of the diffusion coefficients were obtained by fitting the plot of the normalized attenuated signals vs. the term $\gamma^2 g^2 \delta^2 (\Delta - \delta/3)$ to a mono-exponential function.

2.7. Molecular dynamics simulation

The starting coordinates of the DPC micelle–water complex were extracted from simulations performed by Wymore and Gao [47]. Similarly, the initial coordinates of the SDS micelle–water complex were taken from molecular dynamics (MD) simulations performed by MacKerell [48]. The solved NMR structures of C8 in SDS and DPC micelle solutions were used as the starting conformations for the molecular dynamics simulations.

DPC micelles are made up of 65 molecules of DPC with a total charge of 0. The simulation box dimensions were X = 65.26 Å, Y = 65.26 Å, and Z = 65.26 Å. A total of 7752 molecules of water, 28 Cl^- ions and 30 Na^+ ions were added to reach the density of 0.997 g/mL and physiological osmolarity [47]. The peptide's formal charge is −2.

SDS micelles are made up of 60 molecules of SDS with a total formal charge of −60. The simulation box dimensions were X = 70.37 Å, Y = 70.37 Å, and Z = 70.37 Å. A total of 12,560 molecules of water, 12 Cl^- ions and 74 Na^+ ions were added to reach the density of 0.997 g/mL and physiological osmolarity [48].

To generate the initial structure, we applied two different methods: the first method consisted of placing the peptide in the center of the micelle with the two centers of mass overlapping, as described by Kaznessis [49]. To minimize the bumps, the peptide was reduced to half of its size, and the intramolecular forces were scaled down to 10% of the initial values. The system was annealed while the forces were brought back to standard values.

The second method, which we have successfully applied in the past [50,51], consisted of generating hundreds of initial poses in which the peptide's barycenter and orientation are randomly chosen. The configurations were distributed into a newly developed grid [www.yadamp.unisa.it/grimd] to obtain the best starting configuration. The two methods converged into the same initial configuration.

Molecular dynamics simulations were performed using YASARA 12.7.16 [52] with the NPT ensemble at 310 K and 1 atm by coupling the system with a Berendsen thermostat [53] and by controlling the pressure in the manometer pressure control mode. The YAMBER3 force field was used. All simulations ran with a 1.25 fs time step for intramolecular forces and a 2.50 fs time step for intermolecular forces. The equilibration period was 20 ns.

The production run for the C8–DPC micelle system lasted 50 ns, whereas that for the C8–SDS micelles lasted 150 ns.

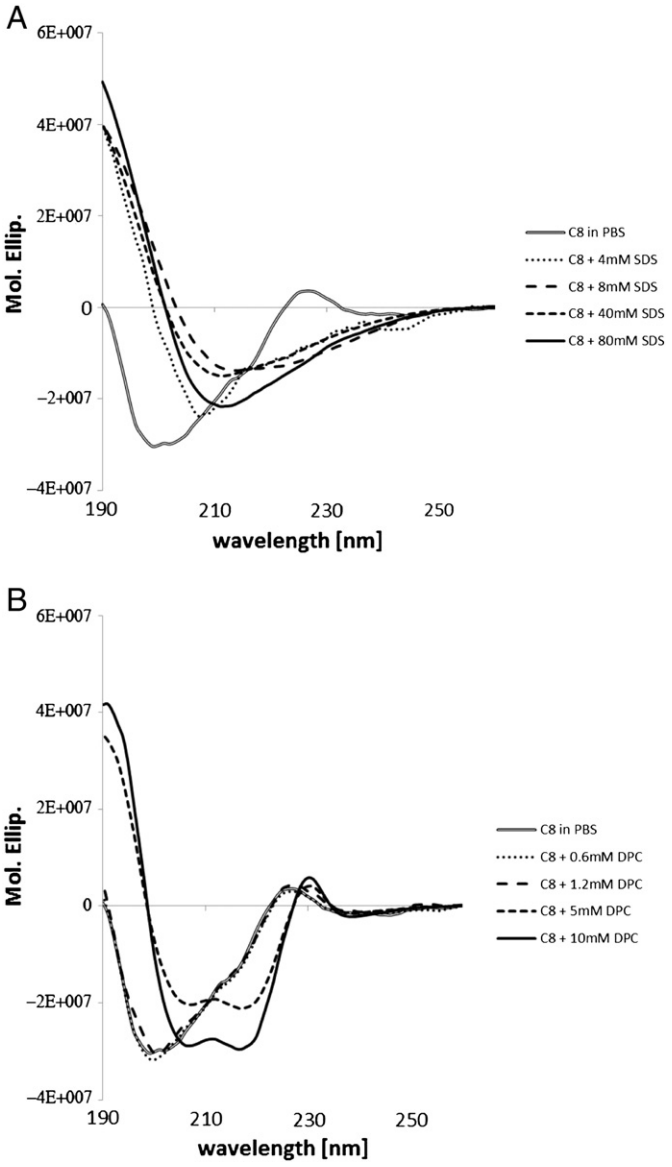

Fig. 1. Normalized circular dichroism spectra of C8 in phosphate buffer and in the presence of increasing concentrations of DPC (A) and SDS (B).

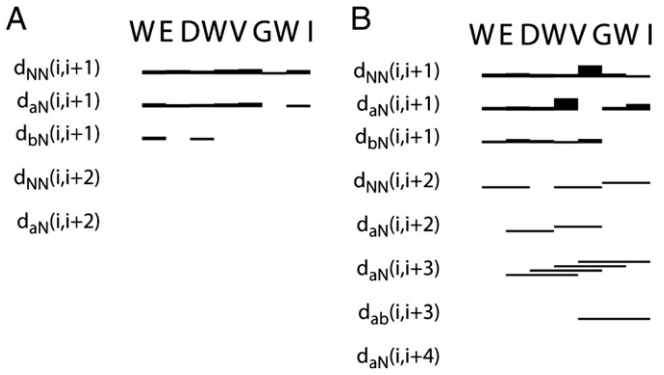

Fig. 2. NOE connectivities from NOESY spectra of C8 in SDS (A) and DPC (B) micelle solutions. Spectra were collected at 600 MHz and 300 K with the following concentrations: C8 peptide, 1 mM; SDS, 80 mM and DPC, 10 mM.

3. Results

3.1. Conformational analysis

3.1.1. CD spectroscopy

The conformation of C8 in DPC and SDS micelles was analyzed by CD spectroscopy. CD spectra were recorded in phosphate buffer (pH 6.8), and phosphate buffer containing increasing amounts of DPC or SDS (Fig. 1).

Quantitative estimation of C8 CD spectra was performed using DICHROWEB website. Both CONTIN and SELCON softwares were used for a validation of the results [33]. CD spectra of C8 recorded at submicellar concentrations of DPC and SDS detergents respectively indicate the coexistence of equally populated conformer families corresponding to β-strands, β-turns and unordered structures. This conformational behavior is mainly conserved at micellar and supramicellar SDS concentrations. At micellar and supramicellar DPC concentrations CD spectra of C8 indicate the prevalence of β-turn structure.

3.1.2. NMR analysis

NMR spectra were recorded on a Bruker DRX-600 spectrometer. ^{1}H monodimensional NMR spectra were recorded in water containing increasing amounts of detergents. At concentrations of SDS and DPC tenfold greater than the c.m.c., 2D COSY, TOCSY and NOESY were recorded to allow chemical shift assignment according to the conventional procedure of Wuthrich [54]. The proton chemical shifts of C8 are reported in the Supplementary data (Tables S1–S2).

Analysis of the chemical shifts revealed significant perturbations in the proton resonances in response to the addition of DPC, whereas less evident chemical shift modifications were observed in response to the addition of SDS.

3.1.3. NMR structure calculation

COSY, TOCSY and NOESY spectra of C8 in DPC and SDS micelles were recorded and analyzed using SPARKY software [38]. Fig. 2 shows a summary of all sequential and medium-range connectivities observed in the NOESY spectra of C8 in DPC and SDS micelle solutions. Fig. 2A shows that minor NOE effects were present in the NOESY spectra of C8 in the SDS micelle solution, indicating the prevalence of disordered and flexible conformations. In contrast, Fig. 2B shows that the NMR spectra of C8 in DPC micelles include regular sequential and medium-range NOEs, consistent with the presence of regular secondary structures.

On the basis of the NOE data, structure calculations for C8 were performed using CYANA software. The NMR structure bundles (Fig. 3) revealed the paucity of ordered structures in SDS (RMSD 0.98), whereas high structural agreement was observed for the NMR structure bundle of C8 in DPC micelle solution (RMSD C8 in DPC: 0.69). Analysis of the backbone torsion angles according to PROMOTIF algorithms [55] indicated the preponderance of type I β-turn conformations involving residues Trp^{1}–Trp^{4}, Glu^{2}–Val^{5} and Val^{5}–Ile^{8} in DPC micelles. In SDS micelles, less regular secondary structures were observed, with a minor presence of γ-turns.

3.2. C8–micelle interactions

3.2.1. Fluorescence titration measurements

Changes in the solvent exposure of the tryptophan residues of C8 due to the peptide's interactions with SDS or DPC micelles were studied by monitoring the Trp fluorescence emission spectra at increasing surfactant concentrations. The fluorescence intensities of some fine vibronic structures in the Trp fluorescence spectrum exhibit strong

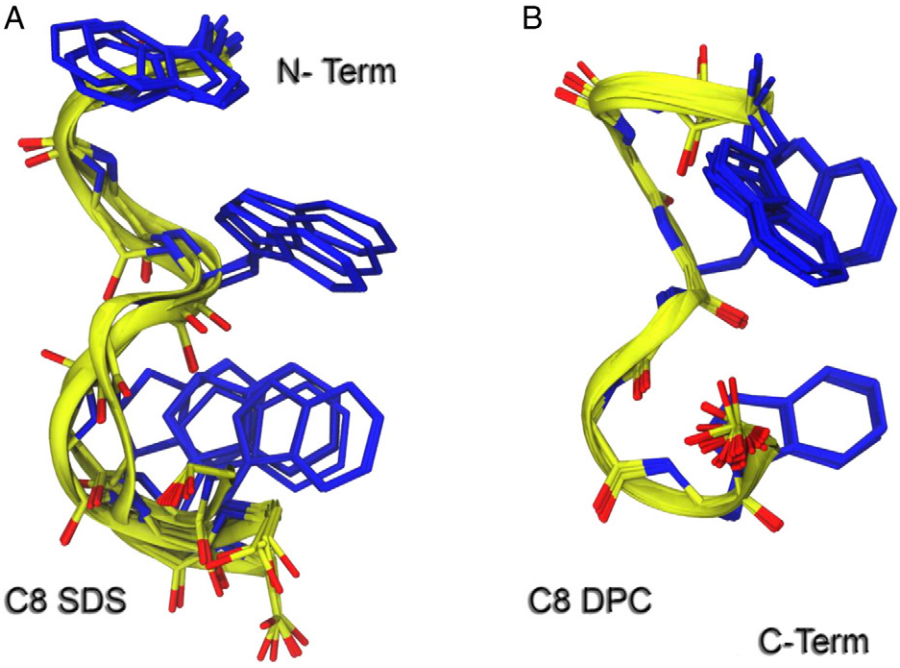

Fig. 3. NMR structure bundles for C8 in SDS (A) and DPC (B) micelle solutions. The structures are overlapped at the level of the backbone.

environmental dependence [56,57] in particular, the emission maximum shifts from 355 to 360 to approximately 330 nm when transitioning from water to an apolar medium. The quantum yield could also undergo large changes, the direction and extent of which depend on the system under consideration [58–60].

The fluorescence spectra of C8 in phosphate buffer indicate that the Trp side chains were fully exposed to the aqueous medium ($\lambda_{max} \approx$ 354 nm). In the presence of DPC micellar aggregates, a dramatic quantum yield increase was observed (Fig. 4B) due to the peptide's interaction with the micelles. However, a limited shift in the emission maximum ($\lambda_{max} \approx$ 345 nm) was observed, thus indicating that the Trp residues of the micelle-interacting peptide move to an environment only slightly more apolar than that of the aqueous solution. This evidence suggests that the peptide was positioned at the micelle interface. To gain quantitative information on the peptide–surfactant interaction, we analyzed the variation in Trp fluorescence for C8 at $\lambda = 354$ nm with changes in the DPC concentration (Fig. 4B). The C8 spectrum remained unperturbed up 0.6 mM, corresponding to the surfactant's c.m.c., indicating an almost negligible interaction between C8 and DPC monomers. Above the c.m.c., the fluorescence steeply increased, quickly reaching a plateau value. When a nonlinear best-fitting procedure was applied to the data according to a previously reported model [26], the apparent peptide–surfactant association constant, K_a, and the number of DPC molecules, *n*, that bind the peptide can be estimated. The obtained results ($K_a = (1.8 \pm 0.3) \times 10^5\ M^{-1}$, $n = 4 \pm 1$) point to a strong C8 interaction with a low number of DPC molecules. Interestingly, these values are slightly lower than those obtained for C8 interacting with POPC liposomes ($K_a = (8.3 \pm 0.6) \times 10^5\ M^{-1}$, $n = 6 \pm 2$) [26]. These lower values could be an effect of the higher curvature of the micelles than the vesicular aggregates.

The fluorescence spectrum of C8 was not significantly modified by the addition of SDS (Fig. 4A and B), indicating that there was minimal perturbation of the Trp hydration upon the interaction of C8 with SDS micelles.

3.2.2. NMR diffusion experiments

Self-diffusion coefficients are useful tools for obtaining structural information about multi-component systems [61,62], as they are closely related to the hydrodynamic radii of the diffusing particles [63]. The self-diffusion coefficients of proteins and peptides depend on self-aggregation phenomena [64,65] and, in micellar solutions, on the interaction with the surfactant aggregates [66–69].

Table 1
Self-diffusion coefficients (D_{obs}) and hydrodynamic radii of SDS and DPC micelles in the presence of the peptide C8. Percentages of calculated C8 bound (Mf_{bound}) to SDS and DPC micelles.

Sample[a]	Peptide diffusion coefficient [10^{-10} m^2 s^{-1}]	Surfactant diffusion coefficient [10^{-10} m^2 s^{-1}]	Hydrodynamic micelle radius [A]
C8 in phosphate buffer	2.85	/	/
C8 in 10 mM DPC	0.85	0.86	22
C8 in 80 mM SDS	0.80	0.82	24
10 mM DPC	/	0.89	21
80 mM SDS	/	0.96	20

[a] Samples were solubilized in 25 mM buffer phosphate at pH 6.8 in D_2O at 302 K.

In the present study, PFG-NMR experiments were first performed on C8 aqueous solutions. The observed peptide diffusion coefficient, $D_{C8} = (2.85 \pm 0.04) \times 10^{-6}$ cm^2 s^{-1}, was quite high, indicating that the peptide exhibited no tendency to self-aggregate.

The peptide self-diffusion coefficients in SDS and DPC micelle solutions, $D_{C8(SDS)}$ and $D_{C8(DPC)}$, are shown in Table 1. They were much lower than that observed in the aqueous solution, suggesting that C8 significantly interacted with both micellar systems. Generally speaking, the self-diffusion coefficient of a peptide in a micellar solution is the weighted average of the coefficients of the free and micelle-bound molecules [66,70] because the free and bound peptides are undergoing fast exchange on the NMR timescale. The diffusion coefficient of free peptide molecules can be assumed to be equal to the peptide diffusion coefficient in aqueous solution after correction for the obstruction of diffusion by the micellar aggregates [66]. In contrast, the diffusion coefficient of the bound peptides coincides with the diffusion coefficient of the micelles, provided that the concentration of the micelles is much higher than the c.m.c. for the particular surfactant [66,71], which is the case for this study. The diffusion coefficient/s of the surfactants in the presence of the peptide, $D_{SDS(C8)}$ and $D_{DPC(C8)}$, are also reported in Table 1. Inspection of the table shows that $D_{C8(SDS)}$ and $D_{C8(DPC)}$ coincided, within the experimental uncertainty, with $D_{SDS(C8)}$ and $D_{DPC(C8)}$. In other words, the peptide molecules diffused together with the surfactant aggregates, and the fraction of free C8 was negligible.

For comparison, measurements were performed on SDS–water and DPC–water binary mixtures at the same SDS and DPC concentrations

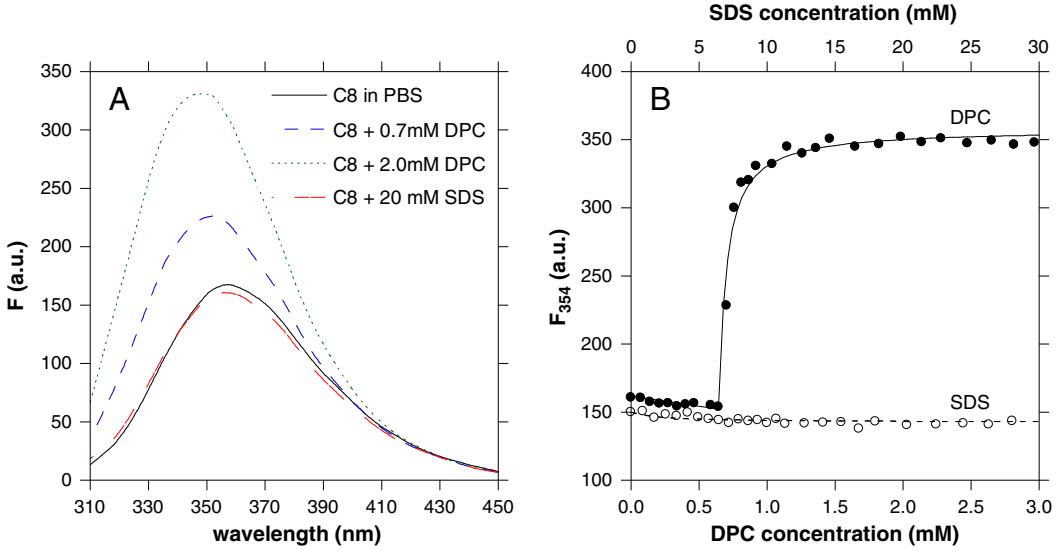

Fig. 4. (A) Fluorescence emission spectra of C8 in phosphate buffer and in the presence of DPC and SDS at the concentrations indicated in the legend. (B) Trp fluorescence variation of C8 at $\lambda = 354$ nm with increasing DPC or SDS concentrations. The solid line shows the data interpolation according to the model cited in the text.

employed to solubilize the polypeptide. The surfactant self-diffusion coefficients obtained in the absence of the peptide, D_{SDS} and D_{DPC}, are shown in Table 1.

Interestingly, $D_{SDS(C8)}$ and $D_{DPC(C8)}$ were lower than D_{SDS} and D_{DPC}. The reduction in the self-diffusion coefficient of DPC was small, whereas this decrease is significant in the case of SDS. The surfactant self-diffusion coefficient (D_{surf}, i.e., D_{SDS} or D_{DPC}) is related to the micelle's dimensions by the Stokes–Einstein relation:

$$R_H = k_B T/(6\pi\eta D_{surf})$$

where R_H is the hydrodynamic radius and η is the viscosity of the aqueous medium. The R_H values reported in Table 1 show that C8 caused a relevant increase in the dimensions of SDS micellar aggregates.

3.2.3. Spin-label studies

To investigate the positioning of the peptide with respect to the surface of the micelles, 5-doxyl-stearic acid paramagnetic probes were used. 5-Doxyl-stearic acid contains a doxyl head group, a cyclic nitroxide with an unpaired electron, that is bound to the aliphatic chain carbon at position 5. Unpaired electrons lead to dramatically accelerated longitudinal and transverse relaxation rates of protons in spatial proximity via highly efficient spin-electron relaxation. Paramagnetic probes are known to induce broadening of the NMR signals and decreases in the resonance intensities of residues close to the surface (5-doxyl) of the micelles [72–75].

TOCSY spectra of C8 in the presence and absence of the spin labels were recorded, keeping all other conditions the same. In the presence of 5-doxyl stearic acid, several NH/CHα signals from the experiments performed in the presence of the spin label were broadened and decreased in intensity relative to those for a control sample without the spin label. Graph shown in Fig. 5 presents the variation in the NH intensities measured for C8 in micelle solutions with or without 5-doxyl stearic acid. In DPC micelles, an evident effect of the spin label was observed, with a drastic reduction in the NH intensities, particularly those for Trp^1, Glu^2, Trp^4 and Trp^5. In SDS micelles, a moderate and non-specific reduction in the NH intensity was evident, with Gly^6 and Ile^8 exhibiting significant perturbations.

3.3. Molecular dynamics simulations

MD simulations of C8 with DPC and SDS micelles at pH 7 were performed to examine the peptide/micelle interactions at the atomic level.

The NMR structures solved for the SDS and DPC micelle solutions were used as the starting conformations, and the initial position of the peptide was determined according to the two protocols described in the Experimental section. In all cases, similar initial configurations were observed: the peptide comes into close contact with the micelle head groups within the first few nanoseconds and equilibrates for the rest of the simulation (up to 50 ns). The fluctuations in the temperature, pressure, density and total energy (potential + kinetic) of the systems at the minimal values were recorded. The backbone root-mean-square deviation (RMSD) values from the initial secondary structures of C8 as a function of time show that the peptide formed transient secondary structures ranging from turn-helix to turn conformations (Supplementary data).

The analysis of the trajectories for C8 in SDS micelles showed that during the first 40 ns of the simulation, C8, which was surrounded by water molecules (10–14 water molecules within 4 Å of the peptide) and two Na^+ ions, binds SDS, inducing changes to the micelle's surface and shape. After 40 ns, the peptide–micelle system undergoes a structural reorganization and changes morphology due to the loss of three SDS molecules and several water molecules. RDF graphs (Supplementary data) showing the radial distribution functions (g(r)) for the backbone

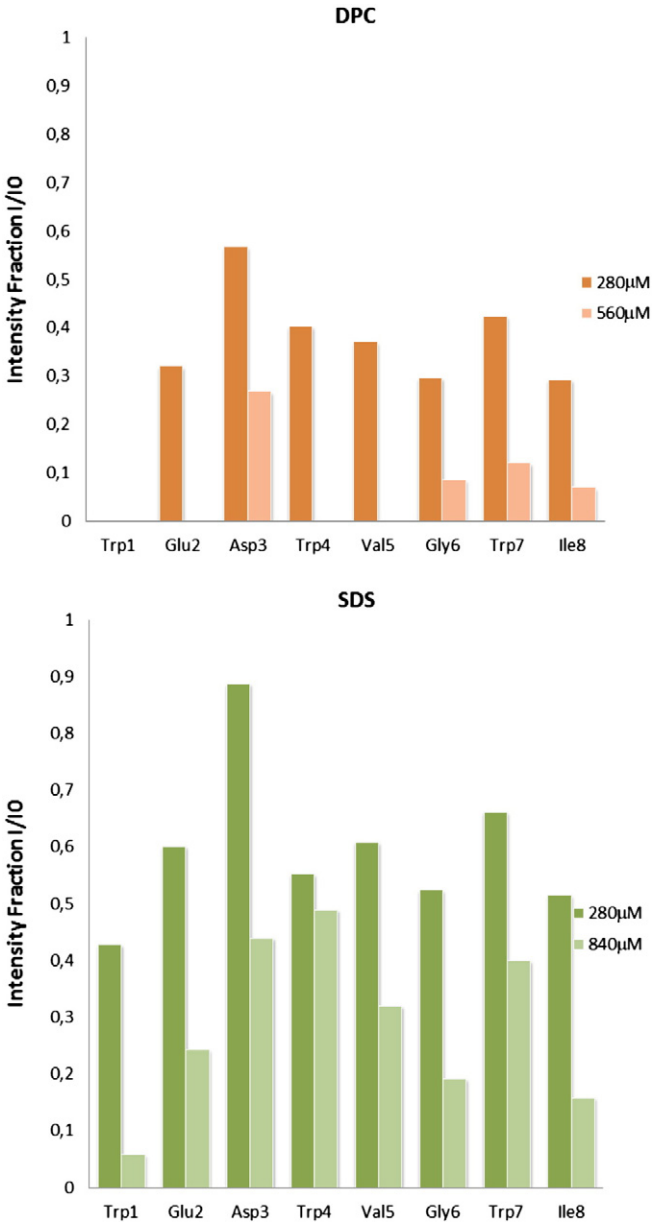

Fig. 5. ^{1}H backbone NH intensities of C8 in DPC and SDS micelles recorded in the absence and the presence of 5-doxyl-stearic acid. Legends in the frames are relative to spin label concentrations.

NHs of the peptide and the C-12 atom of the SDS molecules indicate that C8 is in contact with the inner core of the detergent as a consequence of the destabilization of the micelles (Fig. 6).

In contrast to the SDS micelles, the DPC micelles were not modified upon interaction with the C8 peptide according to the analysis of the trajectory. Both the number of DPC molecules and the spherical symmetry were preserved. C8 interacts strongly with the DPC micelle surface, as demonstrated by the RDF values involving the C8 backbone NHs and the phosphate head groups of DPC (Supplementary data). This interaction has a stabilizing effect, as indicated by the free binding energy of 8.8 kcal/mol. The interaction with DPC micelles involves primarily Trp residues at the expense of the peptide's secondary structure, which is moderately altered to permit the best interactions with the Trp side chains. The peptide remains on the micelle surface, where it maintains greater flexibility and, on average, lower potential energies as compared to C8 in SDS micelles.

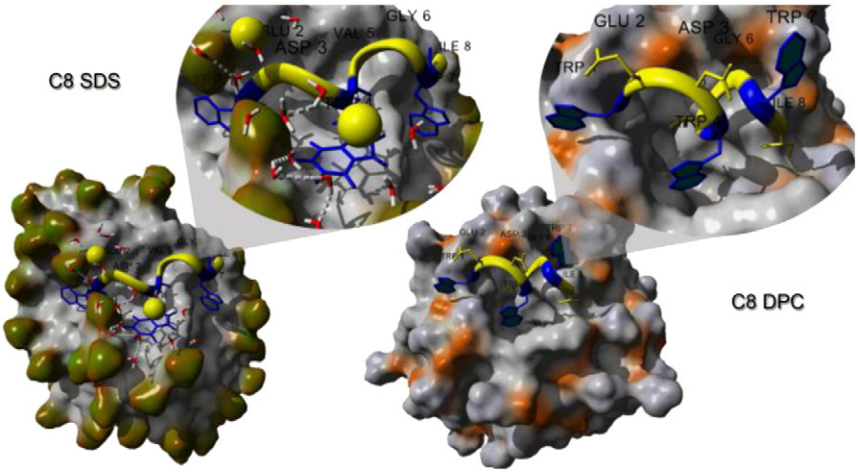

Fig. 6. Binding poses of the fusogenic peptide C8 on DPC and SDS micelles as derived from molecular dynamics calculation of C8 in the micelle–water system. Molecular dynamics simulations were performed using YASARA 12.7.1650, using YAMBER3 force field.

4. Discussion

C8 (Ac-Trp-Glu-Asp-Trp-Val-Gly-Trp-Ile-NH_2), a tryptophan-rich octapeptide modeled on the MPER of gp36 in FIV, exhibits antiviral activity both in vitro and in vivo, resulting from the blocking of the cell entry. The antiviral activity of C8 is related to its tendency to stably reside at membrane interfaces, leading to the destabilization of the bilayer structure [16,17].

To facilitate the design of new molecules able to inhibit virus cell entry that are modeled on the C8 peptide and target FIV MPER, we considered it extremely important to investigate the behavior of C8 at the membrane level. Accordingly, using combined approaches based on fluorescence and EPR spectroscopy, neutron diffraction and molecular dynamics simulation, we have analyzed the ability of C8 to interact with membrane models composed of zwitterionic POPC and DMPC phospholipids [26]. In addition, very recently [29] we investigated on the importance of cholesterol and sphingomyelin in regulating the interaction of the fusogenic peptide C8 with DPPC bilayers. Based on the evidence that the lipid composition is a key factor that fine tunes the physicochemical properties of the membrane [76], contributing to the fusogenic activity of viral proteins [77,78], our previous studies explored the structural behavior of C8 in different bio-membrane systems. These membrane models, although complex and highly bio-mimetic, offered only indirect information about C8's conformational behavior at the membrane level.

High resolution NMR spectroscopy is a suitable method to have the structural coordinates of C8 in membrane mimetic environments, however for a high resolution NMR analysis, membrane mimicking systems are required that tumble sufficiently quickly to produce sharp NMR spectral lines [30,31]. Micelle and bicelle solutions are suitable for these experimental purposes. In particular of the two systems, bicelles have been shown to be better mimics of biological membranes, but may form poor stable solutions and are expensive in the deuterated form. Micelles define an even more simplified model of biological membrane as compared to bicelles and their use is questioned especially due to the curvature of the aggregates. On the contrary they have economic advantages in comparison to bicelles and form stable solution ease to use [79–82]. Based on the reported considerations and in view of the extended exploration of conformational conditions, we decided to use micellar solutions to analyze the conformation of C8. CD and NMR experiments in SDS and DPC micelle solutions chosen as models of negatively charged and zwitterionic membranes, allowed the determination of structural coordinates. Additionally the positioning of C8 on the micelles' surfaces was investigated by collecting Trp fluorescence spectra, PFG-NMR spectra and spin label-aided NMR measurements.

The NMR and CD experiments showed that C8 undergoes to a conformational transition from a random coil to a turn-helical conformation (Fig. 1) when moving from phosphate buffer to micellar concentrations of the zwitterionic surfactant DPC. 3D models calculated on the basis of the NMR data in DPC micelles point to the presence of type I β-turns involving Trp^1–Trp^4, Glu^2–Val^5 and Val^5–Ile^8, with an ordered orientation of the amino acid side chains. Interestingly, the indolyl rings of Trp^1 and Trp^4 define a hydrophobic envelope that interacts with the surface of the zwitterionic DPC micelle, as evident from the Trp fluorescence curves, which show abrupt shifts when DPC micelles are formed (Fig. 4). A selective but evident decrease in the signal intensities induced by 5-doxyl stearic acid (Fig. 5) led to the definition of a map of interactions between C8 and the zwitterionic micellar surface. The evident decrease in the intensities of the backbone NHs belonging to residues Trp^1, Glu^2, Trp^4 and Val^5 shown in Fig. 5 suggests their close proximity to the surface of the micelle. Shallow interactions are evident for the C-terminal residues which appear only weakly susceptible to the presence of the spin labels. These data are in agreement with the results of molecular dynamics simulation obtained in micelle–water system, and point to a structural behavior of C8 similar to that observed in zwitterionic DPPC- or DOPC-bilayers [26].

The NMR data demonstrated conformational flexibility for C8 in the presence of negatively charged SDS micelles. The hydrophobic surface of C8 is less compact in this medium, with the Trp indolyl rings assuming multiple different orientations (Fig. 3). The Trp fluorescence of C8 is imperceptibly affected by SDS micelle formation, indicating the modest exposure of Trp residues to the SDS micelle surface. Consistent with these results, a weak perturbation of the signal intensities was observed in the NMR spectra of C8 acquired in SDS micelles containing 5-doxyl spin labels. The fluorescence data and NMR spectra in the presence of spin labels suggest that there is minimal interaction between C8 and SDS micelles. In contrast to the reported evidence, NMR diffusion experiments indicated that C8 diffuses together with SDS micelles and that C8 binding is able to modify SDS aggregates in terms of shape and dimensions. The molecular dynamics simulation of C8 in a water–SDS micelle system allowed the interpretation of these ambiguous results: in the molecular dynamics simulation of C8 in a water–micelle system, the binding of C8 to the SDS micelle surface surrounded by water molecules is a statistically relevant event. C8, which is hydrated and flexible, induces change to the size and shape of the SDS aggregates, leading to the occasional loss of tensioactive molecules.

The interactions between membrane-active peptides and the membrane surface are primarily mediated by hydrophobic and electrostatic effects [83,84]. C8, having three Trp residues, is highly favored in hydrophobic interactions with phospholipid molecules of membrane surface.

However, C8 also contains Asp^2 and Glu^3, two negatively charged residues; therefore, the tendency of C8 to interact with hydrophobic membranes may be limited due to the electrostatic repulsion between the negative side chains of C8 and the negative sulfate heads of SDS. Two primary driving forces control the interaction between C8 and negatively charged membrane surfaces: the strong hydrophobic interaction due to the three Trp residues and the electrostatic repulsion due to the negatively charged Asp and Glu residues. Our data suggest that to mitigate electrostatic repulsion the peptide surrounds itself with water molecules. The presence of water envelope is demonstrated by i) the fluorescence data showing that Trp is exposed to an aqueous environment and ii) the weak perturbation of the NH NMR signals by the spin labels. Both the diffusion experiments and the molecular dynamics simulations indicate that interaction of C8 with the SDS micelle surface, mediated by water, induces the destabilization of the aggregates, with changes to their shape and dimensions.

Considering the membrane fusion activity of the C8 peptide and its possible analogs and considering the compositions of the virus and cell membranes, characterized by a relevant content of negative charge, our data open the question of which type of structural behavior of a fusion peptide is the most appropriate to obtain membrane fusion. This in turn leads to the question of which condition we should consider for the design of new fusion inhibitors, either (i) the condition characterized by the stable positioning of the peptide on the membrane's surface through hydrophobic interactions or (ii) the more fluid condition in which the peptide hydrated and flexible, interacts in disordered mode with the membrane to induce destabilization. The evaluation of the structural behavior of fusion peptides on membranes with different compositions is in progress to answer this question.

Appendix A. Supplementary data

Supplementary data to this article can be found online at http://dx.doi.org/10.1016/j.bbamem.2013.12.010.

References

[1] S.C. Harrison, Viral membrane fusion, Nat. Struct. Mol. Biol. 15 (2008) 690–698.
[2] M. Lorizate, N. Huarte, A. Saez-Cirion, J.L. Nieva, Interfacial pre-transmembrane domains in viral proteins promoting membrane fusion and fission, Biochim. Biophys. Acta 1778 (2008) 1624–1639.
[3] J.J. Dwyer, K.L. Wilson, D.K. Davison, S.A. Freel, J.E. Seedorff, S.A. Wring, N.A. Tvermoes, T.J. Matthews, M.L. Greenberg, M.K. Delmedico, Design of helical, oligomeric HIV-1 fusion inhibitor peptides with potent activity against enfuvirtide-resistant virus, Proc. Natl. Acad. Sci. U. S. A. 104 (2007) 12772–12777.
[4] L. Cai, M. Gochin, K. Liu, Biochemistry and biophysics of HIV-1 gp41—membrane interactions and implications for HIV-1 envelope protein mediated viral–cell fusion and fusion inhibitor design, Curr. Top. Med. Chem. 11 (2011) 2959–2984.
[5] J. Munch, L. Standker, K. Adermann, A. Schulz, M. Schindler, R. Chinnadurai, S. Pohlmann, C. Chaipan, T. Biet, T. Peters, B. Meyer, D. Wilhelm, H. Lu, W. Jing, S. Jiang, W.G. Forssmann, F. Kirchhoff, Discovery and optimization of a natural HIV-1 entry inhibitor targeting the gp41 fusion peptide, Cell 129 (2007) 263–275.
[6] J. Liu, Y. Deng, Q. Li, A.K. Dey, J.P. Moore, M. Lu, Role of a putative gp41 dimerization domain in human immunodeficiency virus type 1 membrane fusion, J. Virol. 84 (2010) 201–209.
[7] S. Giannecchini, F. Bonci, M. Pistello, D. Matteucci, O. Sichi, P. Rovero, M. Bendinelli, The membrane-proximal tryptophan-rich region in the transmembrane glycoprotein ectodomain of feline immunodeficiency virus is important for cell entry, Virology 320 (2004) 156–166.
[8] J.H. Elder, G.A. Dean, E.A. Hoover, J.A. Hoxie, M.H. Malim, L. Mathes, J.C. Neil, T.W. North, E. Sparger, M.B. Tompkins, W.A. Tompkins, J. Yamamoto, N. Yuhki, N.C. Pedersen, R.H. Miller, Lessons from the cat: feline immunodeficiency virus as a tool to develop intervention strategies against human immunodeficiency virus type 1, AIDS Res. Hum. Retroviruses 14 (1998) 797–801.
[9] B.J. Willett, J.N. Flynn, M.J. Hosie, FIV infection of the domestic cat: an animal model for AIDS, Immunol. Today 18 (1997) 182–189.
[10] G. Pancino, L. Camoin, P. Sonigo, Structural analysis of the principal immunodominant domain of the feline immunodeficiency virus transmembrane glycoprotein, J. Virol. 69 (1995) 2110–2118.
[11] P.F. Serres, Molecular mimicry between the trimeric ectodomain of the transmembrane protein of immunosuppressive lentiviruses (HIV–SIV–FIV) and interleukin 2, C. R. Acad. Sci. III 323 (2000) 1019–1029.
[12] S.C. Frey, E.A. Hoover, J.I. Mullins, Feline immunodeficiency virus cell entry, J. Virol. 75 (2001) 5433–5440.
[13] G. Barbato, E. Bianchi, P. Ingallinella, W.H. Hurni, M.D. Miller, G. Ciliberto, R. Cortese, R. Bazzo, J.W. Shiver, A. Pessi, Structural analysis of the epitope of the anti-HIV antibody 2F5 sheds light into its mechanism of neutralization and HIV fusion, J. Mol. Biol. 330 (2003) 1101–1115.
[14] T. Suarez, S. Nir, F.M. Goni, A. Saez-Cirion, J.L. Nieva, The pre-transmembrane region of the human immunodeficiency virus type-1 glycoprotein: a novel fusogenic sequence, FEBS Lett. 477 (2000) 145–149.
[15] K. Salzwedel, J.T. West, E. Hunter, A conserved tryptophan-rich motif in the membrane-proximal region of the human immunodeficiency virus type 1 gp41 ectodomain is important for Env-mediated fusion and virus infectivity, J. Virol. 73 (1999) 2469–2480.
[16] S. Giannecchini, M.C. Alcaro, P. Isola, O. Sichi, M. Pistello, A.M. Papini, P. Rovero, M. Bendinelli, Feline immunodeficiency virus plasma load reduction by a retroinverso octapeptide reproducing the Trp-rich motif of the transmembrane glycoprotein, Antivir. Ther. 10 (2005) 671–680.
[17] S. Giannecchini, A. Di Fenza, A.M. D'Ursi, D. Matteucci, P. Rovero, M. Bendinelli, Antiviral activity and conformational features of an octapeptide derived from the membrane-proximal ectodomain of the feline immunodeficiency virus transmembrane glycoprotein, J. Virol. 77 (2003) 3724–3733.
[18] S. Lombardi, C. Massi, E. Indino, C. La Rosa, P. Mazzetti, M.L. Falcone, P. Rovero, A. Fissi, O. Pieroni, P. Bandecchi, F. Esposito, F. Tozzini, M. Bendinelli, C. Garzelli, Inhibition of feline immunodeficiency virus infection in vitro by envelope glycoprotein synthetic peptides, Virology 220 (1996) 274–284.
[19] A.M. D'Ursi, S. Giannecchini, A. Di Fenza, C. Esposito, M.R. Armenante, A. Carotenuto, M. Bendinelli, P. Rovero, Retroinverso analogue of the antiviral octapeptide C8 inhibits feline immunodeficiency virus in serum, J. Med. Chem. 46 (2003) 1807–1810.
[20] A.M. D'Ursi, S. Giannecchini, C. Esposito, M.C. Alcaro, O. Sichi, M.R. Armenante, A. Carotenuto, A.M. Papini, M. Bendinelli, P. Rovero, Development of antiviral fusion inhibitors: short modified peptides derived from the transmembrane glycoprotein of feline immunodeficiency virus, Chembiochem 7 (2006) 774–779.
[21] A.B. Williams, New horizons: antiretroviral therapy in 1997, J. Assoc. Nurses AIDS Care 8 (1997) 26–38.
[22] P. Yeni, Update on HAART in HIV, J. Hepatol. 44 (2006) S100–S103.
[23] A.F. Aghokeng, A. Ayouba, E. Mpoudi-Ngole, S. Loul, F. Liegeois, E. Delaporte, M. Peeters, Extensive survey on the prevalence and genetic diversity of SIVs in primate bushmeat provides insights into risks for potential new cross-species transmissions, Infect. Genet. Evol. 10 (2010) 386–396.
[24] C. Esposito, G. D'Errico, M.R. Armenante, S. Giannecchini, M. Bendinelli, P. Rovero, A.M. D'Ursi, Physicochemical characterization of a peptide deriving from the glycoprotein gp36 of the feline immunodeficiency virus and its lipoylated analogue in micellar systems, Biochim. Biophys. Acta 1758 (2006) 1653–1661.
[25] S. Giannecchini, A.M. D'Ursi, C. Esposito, M. Scrima, E. Zabogli, G. Freer, P. Rovero, M. Bendinelli, Antibodies generated in cats by a lipopeptide reproducing the membrane-proximal external region of the feline immunodeficiency virus transmembrane enhance virus infectivity, Clin. Vaccine Immunol. 14 (2007) 944–951.
[26] A. Merlino, G. Vitiello, M. Grimaldi, F. Sica, E. Busi, R. Basosi, A.M. D'Ursi, G. Fragneto, L. Paduano, G. D'Errico, Destabilization of lipid membranes by a peptide derived from glycoprotein gp36 of feline immunodeficiency virus: a combined molecular dynamics/experimental study, J. Phys. Chem. B 116 (2011) 401–412.
[27] G. D'Errico, G. Vitiello, A.M. D'Ursi, D. Marsh, Interaction of short modified peptides deriving from glycoprotein gp36 of feline immunodeficiency virus with phospholipid membranes, Eur. Biophys. J. 38 (2009) 873–882.
[28] S.G. Peisajovich, S.A. Gallo, R. Blumenthal, Y. Shai, C-terminal octylation rescues an inactive T20 mutant implications for the mechanism of HIV/simian immunodeficiency virus-induced membrane fusion, J. Biol. Chem. 278 (2003) 21012–21017.
[29] G. Vitiello, G. Fragneto, A.A. Petruk, A. Falanga, S. Galdiero, A.M. D'Ursi, A. Merlino, G. D'Errico, Cholesterol modulates the fusogenic activity of a membranotropic domain of the FIV glycoprotein gp36, Soft Matter 9 (2013) 6442–6456.
[30] F. Porcelli, R. Verardi, L. Shi, K.A. Henzler-Wildman, A. Ramamoorthy, G. Veglia, NMR structure of the cathelicidin-derived human antimicrobial peptide LL-37 in dodecylphosphocholine micelles†, Biochemistry 47 (2008) 5565–5572.
[31] M. Grimaldi, M. Scrima, C. Esposito, G. Vitiello, A. Ramunno, V. Limongelli, G. D'Errico, E. Novellino, A.M. D'Ursi, Membrane charge dependent states of the beta-amyloid fragment Abeta (16–35) with differently charged micelle aggregates, Biochim. Biophys. Acta 1798 (2010) 660–671.
[32] S.M. Kelly, T.J. Jess, N.C. Price, How to study proteins by circular dichroism, Biochim. Biophys. Acta 1751 (2005) 119–139.
[33] L. Whitmore, B.A. Wallace, DICHROWEB, an online server for protein secondary structure analyses from circular dichroism spectroscopic data, Nucleic Acids Res. 32 (2004) W668–W673.
[34] U. Piantini, O. Sorensen, R.R. Ernst, Multiple quantum filters for elucidating NMR coupling networks, J. Am. Chem. Soc. 104 (1982) 6800–6801.
[35] A. Bax, D.G. Davis, MLEV-17-based two-dimensional homonuclear magnetization transfer spectroscopy, J. Magn. Reson. 65 (1985) 355–360.
[36] J. Jeener, B. Meier, P. Bachmann, R.R. Ernst, Investigation of exchange processes by two-dimensional NMR spectroscopy, J. Chem. Phys. 71 (1979) 4546.
[37] M. Piotto, V. Saudek, V. Sklenář, Gradient-tailored excitation for single-quantum NMR spectroscopy of aqueous solutions, J. Biomol. NMR 2 (1992) 661–665.
[38] T. Goddard, D. Kneller, SPARKY 3, University of California, San Francisco, 2004.
[39] P. Güntert, C. Mumenthaler, K. Wüthrich, Torsion angle dynamics for NMR structure calculation with the new program D1, J. Mol. Biol. 273 (1997) 283–298.
[40] D.A. Pearlman, D.A. Case, J.W. Caldwell, W.S. Ross, T.E. Cheatham, S. DeBolt, D. Ferguson, G. Seibel, P. Kollman, AMBER, a package of computer programs for applying molecular mechanics, normal mode analysis, molecular dynamics and free energy calculations to simulate the structural and energetic properties of molecules, Comput. Phys. Commun. 91 (1995) 1–41.

[41] D.A. Case, D.A. Pearlman, J.W. Caldwell, T.E. Cheatham III, J. Wang, W.S. Ross, C. Simmerling, T. Darden, K.M. Merz, R.V. Stanton, AMBER 7, University of California, San Francisco, 2002.
[42] D. Wu, A. Chen, C.S. Johnson, An improved diffusion-ordered spectroscopy experiment incorporating bipolar-gradient pulses, J. Magn. Reson., Ser. A 115 (1995) 260–264.
[43] K.F. Morris, C.S. Johnson Jr., Diffusion-ordered two-dimensional nuclear magnetic resonance spectroscopy, J. Am. Chem. Soc. 114 (1992) 3139–3141.
[44] G. Vitiello, D. Ciccarelli, O. Ortona, G. D'Errico, Microstructural characterization of lysophosphatidylcholine micellar aggregates: the structural basis for their use as biomembrane mimics, J. Coll. Int. Sci. 336 (2009) 827–833.
[45] P. Stilbs, Fourier transform pulsed-gradient spin-echo studies of molecular diffusion, Prog. Nucl. Magn. Reson. Spectrosc. 19 (1987) 1–45.
[46] J. Tanner, Use of the stimulated echo in NMR diffusion studies, J. Chem. Phys. 52 (1970) 2523.
[47] T. Wymore, X. Gao, T. Wong, Molecular dynamics simulation of the structure and dynamics of a dodecylphosphocholine micelle in aqueous solution, J. Mol. Struct. 485 (1999) 195–210.
[48] A.D. MacKerell Jr., Molecular dynamics simulation analysis of a sodium dodecyl sulfate micelle in aqueous solution: decreased fluidity of the micelle hydrocarbon interior, J. Phys. Chem. 99 (1995) 1846–1855.
[49] A. Langham, Y.N. Kaznessis, Molecular simulations of antimicrobial peptides, Methods Mol. Biol. 618 (2010) 267–285.
[50] I. Gombos, T. Crul, S. Piotto, B. Gungor, Z. Torok, G. Balogh, M. Peter, J.P. Slotte, F. Campana, A.M. Pilbat, A. Hunya, N. Toth, Z. Literati-Nagy, L. Vigh Jr., A. Glatz, M. Brameshuber, G.J. Schutz, A. Hevener, M.A. Febbraio, I. Horvath, L. Vigh, Membrane-lipid therapy in operation: the HSP co-inducer BGP-15 activates stress signal transduction pathways by remodeling plasma membrane rafts, PLoS One 6 (2011) e28818.
[51] T. Crul, N. Toth, S. Piotto, P. Literati-Nagy, K. Tory, P. Haldimann, B. Kalmar, L. Greensmith, Z. Torok, G. Balogh, I. Gombos, F. Campana, S. Concilio, F. Gallyas, G. Nagy, Z. Berente, B. Gungor, M. Peter, A. Glatz, A. Hunya, Z. Literati-Nagy, L. Vigh, Jr., F. Hoogstra-Berends, A. Heeres, I. Kuipers, L. Loen, J.P. Seerden, D. Zhang, R.A. Meijering, R.H. Henning, B.J. Brundel, H.H. Kampinga, L. Koranyi, Z. Szilvassy, J. Mandl, B. Sumegi, M.A. Febbraio, I. Horvath, P.L. Hooper, L. Vigh, Hydroximic acid derivatives: pleiotropic hsp co-inducers restoring homeostasis and robustness, Curr. Pharm. Des. 19 309–346.
[52] E. Krieger, T. Darden, S.B. Nabuurs, A. Finkelstein, G. Vriend, Making optimal use of empirical energy functions: force-field parameterization in crystal space, Proteins Struct. Funct. Bioinforma. 57 (2004) 678–683.
[53] H.J.C. Berendsen, J.P.M. Postma, W.F. van Gunsteren, A. Di Nola, J.R. Haak, Molecular dynamics with coupling to an external bath, J. Chem. Phys. 81 (1984) 3684–3689.
[54] K. Wuthrich, NMR of Proteins and Nucleic Acids, Wiley, 1986.
[55] E.G. Hutchinson, J.M. Thornton, PROMOTIF—a program to identify and analyze structural motifs in proteins, Protein Sci. 5 (1996) 212–220.
[56] S.V. Konev, S. Udenfriend, Fluorescence and Phosphorescence of Proteins and Nucleic Acids, Plenum Press, New York, 1967.
[57] L. Ambrosone, G. D'Errico, R. Ragone, Interaction of tryptophan and N-acetyltryptophanamide with dodecylpentaoxyethyleneglycol ether micelles, Spectrochim. Acta A Mol. Biomol. Spectrosc. 53 (1997) 1615–1620.
[58] P.R. Callis, T. Liu, Quantitative prediction of fluorescence quantum yields for tryptophan in proteins, J. Phys. Chem. B 108 (2004) 4248–4259.
[59] S. Galdiero, A. Falanga, G. Vitiello, M. Vitiello, C. Pedone, G. D'Errico, M. Galdiero, Role of membranotropic sequences from herpes simplex virus type I glycoproteins B and H in the fusion process, Biochim. Biophys. Acta Biomembr. 1798 (2010) 579–591.
[60] A. Falanga, R. Tarallo, G. Vitiello, M. Vitiello, E. Perillo, M. Cantisani, G. D'Errico, M. Galdiero, S. Galdiero, Biophysical characterization and membrane interaction of the two fusion loops of glycoprotein B from herpes simplex type I virus, PloS one 7 (2012) e32186.
[61] Y. Cohen, L. Avram, L. Frish, Diffusion NMR spectroscopy in supramolecular and combinatorial chemistry: an old parameter—new insights, Angew. Chem. Int. Ed. Engl. 44 (2005) 520–554.
[62] G. D'Errico, On the segregative tendency of ethoxylated surfactants in nonionic mixed micelles, Langmuir 27 (2011) 3317–3323.
[63] K.F. Morris, P. Stilbs, C.S. Johnson Jr., Analysis of mixtures based on molecular size and hydrophobicity by means of diffusion-ordered 2D NMR, Anal. Chem. 66 (1994) 211–215.
[64] S.L. Mansfield, D.A. Jayawickrama, J.S. Timmons, C.K. Larive, Measurement of peptide aggregation with pulsed-field gradient nuclear magnetic resonance spectroscopy, Biochim. Biophys. Acta 1382 (1998) 257–265.
[65] A. Dehner, H. Kessler, Diffusion NMR spectroscopy: folding and aggregation of domains in p53, Chembiochem 6 (2005) 1550–1565.
[66] X. Gao, T.C. Wong, Studies of the binding and structure of adrenocorticotropin peptides in membrane mimics by NMR spectroscopy and pulsed-field gradient diffusion, Biophys. J. 74 (1998) 1871–1888.
[67] S. Albrizio, G. Caliendo, G. D'Errico, E. Novellino, P. Rovero, A.M. D'Ursi, Galphas protein C-terminal alpha-helix at the interface: does the plasma membrane play a critical role in the Galphas protein functionality? J. Pept. Sci. 11 (2005) 617–626.
[68] A. Chen, D. Wu, C.S.J. Johnson, Determination of the binding isotherm and size of the bovine serum albumin-sodium dodecyl sulfate complex by diffusion-ordered 2D NMR, J. Phys. Chem. 99 (1995) 828–834.
[69] B. Orioni, M. Roversi, C. La Mesa, F. Asaro, G. Pellizer, G. D'Errico, Polymorphic behavior in protein–surfactant mixtures: the water–bovine serum albumin–sodium taurodeoxycholate system, J. Phys. Chem. B 110 (2006) 12129–12140.
[70] P. Stilbs, Fourier transform NMR pulsed-gradient spin-echo (FT-PGSE) self-diffusion measurements of solubilization equilibria in SDS solutions, J. Colloid Interface Sci. 87 (1982) 385–394.
[71] O. Annunziata, L. Costantino, G. D'Errico, L. Paduano, V.V. Vitagliano, Transport properties for aqueous sodium sulfonate surfactants, J. Colloid Interface Sci. 216 (1999) 16–24.
[72] R. Bader, A. Bettio, A.G. Beck-Sickinger, O. Zerbe, Structure and dynamics of micelle-bound neuropeptide Y: comparison with unligated NPY and implications for receptor selection, J. Mol. Biol. 305 (2001) 307–329.
[73] I. Solomon, Relaxation processes in a system of two spins, Phys. Rev. 99 (1955) 559.
[74] C. Esposito, M. Scrima, A. Carotenuto, A. Tedeschi, P. Rovero, G. D'Errico, A.M. Malfitano, M. Bifulco, A.M. D'Ursi, Structures and micelle locations of the nonlipidated and lipidated C-terminal membrane anchor of 2′,3′-cyclic nucleotide-3′-phosphodiesterase, Biochemistry 47 (2008) 308–319.
[75] S. Pandey, M.C. Alcaro, M. Scrima, E. Peroni, I. Paolini, S. Di Marino, F. Barbetti, A. Carotenuto, E. Novellino, A.M. Papini, A.M. D'Ursi, P. Rovero, Conformational study of a peptide derived from glycoprotein gp36 of feline immunodeficiency virus, J. Med. Chem. 55 (23) (2012) 10437–10447.
[76] L.J. Pike, The challenge of lipid rafts, J. Lipid Res. 50 (2009) S323–S328.
[77] H. Aizaki, K. Morikawa, M. Fukasawa, H. Hara, Y. Inoue, H. Tani, K. Saito, M. Nishijima, K. Hanada, Y. Matsuura, Critical role of virion-associated cholesterol and sphingolipid in hepatitis C virus infection, J. Virol. 82 (2008) 5715–5724.
[78] V.I. Razinkov, F.S. Cohen, Sterols and sphingolipids strongly affect the growth of fusion pores induced by the hemagglutinin of influenza virus, Biochemistry 39 (2000) 13462–13468.
[79] W. Surya, Y. Li, O. Millet, T. Diercks, J. Torres, Transmembrane and juxtamembrane structure of alphaL integrin in bicelles, PloS one 8 (2013) e74281.
[80] O. Vinogradova, T. Haas, E.F. Plow, J. Qin, A structural basis for integrin activation by the cytoplasmic tail of the alpha IIb-subunit, Proc. Natl. Acad. Sci. U. S. A. 97 (2000) 1450–1455.
[81] O. Vinogradova, A. Velyvis, A. Velyviene, B. Hu, T. Haas, E. Plow, J. Qin, A structural mechanism of integrin alpha(IIb)beta(3) "inside-out" activation as regulated by its cytoplasmic face, Cell 110 (2002) 587–597.
[82] R. Mannhold, H. Kubinyi, G. Folkers, O. Zerbe, BioNMR in Drug Research, Wiley-VCH, 2006.
[83] A.J. de Jesus, T.W. Allen, The role of tryptophan side chains in membrane protein anchoring and hydrophobic mismatch, Biochim. Biophys. Acta 1828 (2013) 864–876.
[84] D.I. Chan, E.J. Prenner, H.J. Vogel, Tryptophan- and arginine-rich antimicrobial peptides: structures and mechanisms of action, Biochim. Biophys. Acta 1758 (2006) 1184–1202.